Condensed Phase Diagrams for the Metal–W–S Systems and Their Relevance for Contacts to WS_2

Yitian Zeng[a], Anna Domask[a], Suzanne Mohney[a,*]

[a]*Department of Materials Science and Engineering, The Pennsylvania State University, University Park, PA 16802, United States*

Abstract

Motivated by interest in contacts to the layered semiconductor WS_2, this study investigates condensed phase equilibria in M–W–S systems (M = transition or post-transition metal) and relates the findings to earlier work on M–Mo–W systems. Thermodynamic data were collected or estimated for the binary phases bearing M, W, and/or S; and a literature search for existing ternary phases was performed. Condensed phase M–W–S isothermal phase diagrams were calculated where sufficient data was available. These phase diagrams reflected three general forms. The early transition metals and group 13 post-transition metals were mostly reactive with WS_2, with the resulting diagrams being either metal sulfide dominant or ternary/solid solution dominant. The late transition metals were all WS_2 dominant, where the metal is in equilibrium with WS_2. These findings are similar to those from our earlier study on the M–Mo–S phase diagrams and can be used to guide studies on contacts to WS_2.

Keywords WS_2, phase equilibria, phase diagram, contact, transition metal dichalcogenide

1. Introduction

Tungsten disulfide is a layered transition metal dichalcogenide (TMD) semiconductor that has long been studied for electronics [1,2] , lubrication [3,4] and catalysis [5,6]. Novel electronic properties that arise as these materials thin to a single or a few layers thick make them particularly attractive for

*Corresponding author email: mohney@ems.psu.edu

application in next-generation electronics, photonics, and optoelectronics [7–9]. MoS_2 and WS_2 are similar: they both exhibit a trigonal prismatic structure, are van der Waals layered solids, and have an indirect bandgap in the bulk that becomes a direct bandgap in monolayer films [10]. While many of the properties of WS_2 and MoS_2 are very similar, a few key differences are emerging. The photoluminescence intensity of the edges of monolayer WS_2 is 20 times higher than that from monolayer MoS_2 [11,12], and monolayer WS_2 MOSFETs have higher theoretical ballistic performance than MoX_2 (X = S, Se, and Te) [13]. Besides, the Fermi-level pining of WS_2 is close to the middle of the bandgap, making it desirable for ambipolar conduction in field effect transistors (FETs) [8,14].

For electronic applications, the interactions between TMDs and transition metals are of great importance because contact metallurgy for TMDs influences the performance of electronic devices. Recent investigation by Hwang et al. [14] showed that Ti/Au contacts to few-layer WS_2 exhibit Schottky behavior, which made extraction of device parameters more challenging; historically, Ag paint/epoxy and a Ga−In eutectic were reported to be Ohmic contacts to bulk WS_2 [15]. This paper expands upon our earlier work predicting and discussing transition metal (M)–MoS_2 interactions and M–Mo–S ternary phase diagrams, as described in Domask et al. [16]. Using a similar approach, we studied the M–W–S systems, where M is a metal from group 4 to group 13, and we draw comparisons between the interaction of metals with MoS_2 and WS_2. Although there could be some differences in the phase equilibria for nanoscale materials, the bulk phase diagrams we have calculated and compiled can still inform future research on contacts to single and few-layer WS_2.

2. Procedures

2.1. Source of Thermodynamic Data

In this study, we calculated 17 M–W–S ternary phase diagrams at room temperature (298 K) based on published thermodynamic data, where M = Zr, Cr, Mn, Fe, Ru, Os, Co, Rh, Ni, Pd, Pt, Cu, Ag,

Au, Hg, Al, and Ga. The majority of the thermodynamic data for the M–S compounds were from two sources: *Materials Thermochemistry* by Kubaschewski [17] and *Thermodynamic Data for Inorganic Sulphides, Selenides and Tellurides* by K.C. Mills [18]. Thermodynamic data for the M–W phases in a few cases were obtained using Miedema's method from *Cohesion in Metals: Transition Metal Alloys* by de Boer [19]. Where additional papers from the literature were consulted for some phases, they are cited in the appropriate section. All of the thermodynamic data used in this paper are tabulated in Appendix I.

The frequently cited W–S binary phase diagram by Vogel et al. [20]—which is included in the *Binary Alloy Phase Diagrams* [21]—shows two room-temperature, intermetallic compounds: WS_2 and WS_3. While the existence of WS_2 as a stable, room-temperature intermetallic compound is well known, the thermodynamic stability of WS_3 at room temperature is not agreed upon. Experiments by Ŝtemprok et al. investigating the sulfur-rich portion of the W–S system concluded that WS_2 was the only phase that coexisted with sulfur, and they never synthesized WS_3 [22]. Wildervanck et al. carefully prepared WS_3 via three different methods under nitrogen to prevent contamination, as described in [23]. When analyzed via X-ray diffraction, the WS_3 was entirely amorphous. They also discussed how previously reported X-ray diffraction patterns for "crystalline WS_3" were likely of a W–S–O compound, due to oxygen contamination, since WS_3 is very sensitive to oxygen [23]. Voorhoeve et al. also conducted experiments that indicated that WS_3 was an amorphous, metastable W–S phase [24]. Therefore, this paper will consider only one binary W–S phase, WS_2. The Gibbs free energy of formation of WS_2 at 298 K used in this study is −249.9 kJ/mol [17].

Ternary phases have been reported in the Hf–W–S, Nb–W–S, Ta–W–S, and In–W–S systems at moderate temperatures: Hf_9W_4S [25]; Nb_3WS_8 [26]; $Nb_7W_{26}S_{67}$ [27]; $Ta_{33}WS_{66}$ [27]; $Ta_{25}W_8S_{67}$ [27], and In_xWS_2 ($0 \leq x \leq 1$) [28]. $Cu_{12}W_{29}S_{59}$ and $Ag_{12}W_{29}S_{59}$ are also listed in the *Handbook of Ternary Alloy Phase Diagrams* [29] but are believed to be metastable solid solutions of the metals in WS_2 and are not stable ternary phases [30]. Note that there are many fewer reported ternary phases in the M–W–S systems

than in the M–Mo–S systems [16], and attempts to produce some of the analogues of the ubiquitous M–Mo–S Chevrel phases using W have been unsuccessful [31].

2.2. Ternary Diagram Calculations

Using the sources of thermodynamic data described above, we calculated the Gibb's free energy of reaction (ΔG°_{rxn}) for pairs of phases as reactants and other pairs of phases as products, whenever crossing tie-lines could be drawn. Only pairs of phases that were thermodynamically stable against forming any of the possible pairs of products were accepted as stable tie-lines. The ternary phase diagrams were calculated at 298 K, and intermetallic phases were treated as line compounds. When the entropy of formation of an intermetallic phase was not available, this study assumed it to be zero, which is reasonable because the entropy of formation is typically small for condensed phases formed from other condensed phases. Although our calculations are for 298 K, it is not unusual for such ternary phase diagrams involving metals and semiconducting binary compounds to remain useful for making predictions about annealed contacts, since we are considering phase equilibria among only condensed phases. The calculation is also described in our recent work on the metal–Mo–S systems [16].

Solid solubility of W in M was treated in our calculations when the solubility of W was larger than a few percent (M = Ru, Os, Rh, Pd, and Pt). Application of the regular solid solution model estimated the enthalpy and entropy of mixing (ΔH_{mix} and ΔS_{mix}, respectively) in a M–W system, where

$$\Delta H_{\mathrm{mix}} = I_{\mathrm{MW}} x_{\mathrm{M}} x_{\mathrm{W}}$$

and

$$\Delta S_{\mathrm{mix}} = -\mathrm{R}(x_{\mathrm{M}} \ln x_{\mathrm{M}} + x_{\mathrm{W}} \ln x_{\mathrm{W}}),$$

where I_{MW} is a composition invariant interaction energy estimated in [19], x_{M} is the mole fraction of metal, and x_{W} is the mole fraction of tungsten. Since many of the binary M–W phase diagrams we found

were available only for high temperatures (T > 1273 K), the extent of solubility of W in M was taken from the lowest temperature shown on the binary phase diagram. We furthermore neglected the difference in the equilibrium crystal structure between M and W, if different, and hence any change in free energy required to convert body-centered cubic W to the crystal structure of M. This simple approach overestimates the thermodynamic stability of the M–W solid solution. Nevertheless, the inclusion of solid solubility in our calculations did not alter any of the tie-lines we found compared to when we neglected it, and is not important for us to consider further.

This study also displays unstable tie-lines when the Gibbs free energy of reaction (ΔG°_{rxn}) was less than 8 kJ/(mol of atoms), adopted from our previous work [16,32,33]. In a related study of M–Ga–Sb systems [33], incorrect tie-lines compared to experimental findings were identified for several predictions that were made within a margin of error of 3 kJ/(mol of atoms). In addition, the uncertainty in the free energies of formation that we selected for the present work, whenever error bars were explicitly reported, was less than 8 kJ/(mol of atoms), except for the Ti–S and V–S phases. (Due to considerable uncertainties in the Ti/V–S binary systems, we did not draw ternary diagrams involving these metals.) Although there were some M–W phases for which we estimated the enthalpy of formation using Miedema's method, and even approximated the entropy of formation to be zero, these free energies of formation were small negative values, so the selected error of 8 kJ/(mol of atoms) as the threshold to call out marginally unstable tie-lines remains reasonable. Indicated by dashed lines on the ternary phase diagrams, such marginally unstable tie-lines were found in the Zr–, Cr–, Fe–, Co–, Rh–, and Ni–W–S ternary systems, and their presence reflects uncertainty involving particular tie-lines in our predictions for these systems.

3. Results and Discussion

The calculated and published ternary phase diagrams for the M–W–S systems are categorized into 3 types: metal-sulfide dominant, solid solution/ternary phase dominant, and WS_2 dominant. A summary of these results can be found in Figure 1.

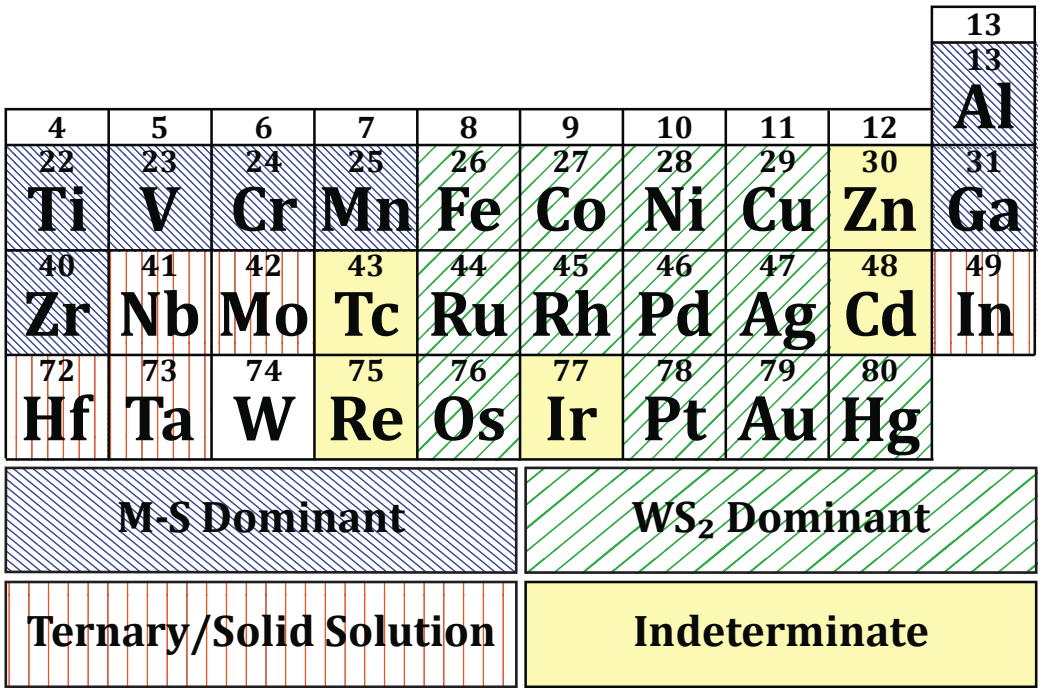

Fig 1. Periodic table summarizing phase diagrams of the M–W–S ternary systems at 298 K. Ternary phase diagrams were calculated at room temperature for all systems labeled "WS_2 Dominant" and "M–S Dominant". The systems noted as "Ternary/Solid Solution" have either ternary or solid solution phases reported in the literature. Phase diagrams of these systems were not calculated, but the published Mo–W–S ternary phase diagram at 773 K was used [34]. The systems marked "Indeterminate" lacked sufficient information for any conclusion to be drawn. Information in the Ti and V systems is more limited, so their ternary phase diagrams are not presented in this study.

A metal-sulfide dominant phase diagram, schematically depicted in Figure 2a, shows a phase diagram dominated by one or more M–S phases. This type of phase diagram was found in the Zr, Cr, Mn, Al, and Ga diagrams calculated for 298 K. (Fe and Cu at 1000 K also exhibit this type of phase diagram.) If one uses the limited information available regarding their interactions with sulfur, Ti and V may also exhibit this type of diagram. No M–W dominant phase diagram was found in this study.

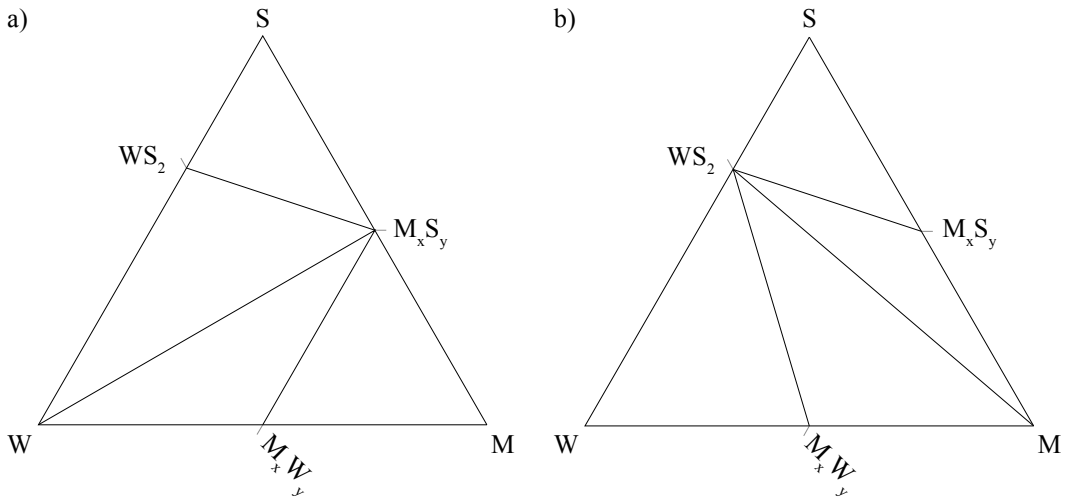

Fig 2. Hypothetical (a) M–S dominant phase diagram showing the tie lines emanating from a metal sulfide to WS_2, W metal, and a M–W phase, and (b) WS_2 dominant phase diagram showing the tie lines emanating from WS_2 to a metal sulfide, metal, and a M–W phase.

A solid solution and/or ternary phase(s) is (are) present in the phase diagram (M = Hf, Nb, Ta, Mo, and In). For a few of the early transition metals close to W on the periodic table (M = Nb, Ta, and Mo), MS_2 and WS_2 form layered solid solutions ($M_xW_{1-x}S_2$), where M or W occupy the metal sublattice and the S remains on its own sublattice [27,34]. Similarly, In intercalates into the van der Waals gap of WS_2 up to 25 at.% In [28]. There are also ternary phases (Hf_9W_4S, Nb_3WS_8) that have distinct crystal structures from WS_2 [25,26,35]. There is insufficient thermodynamic data available to calculate a ternary phase diagram for any of these systems. However, if the ternary phases in the Hf–W–S system are ignored, its phase diagram is predicted to be metal-sulfide dominant.

The WS_2 dominant phase diagram shown in Figure 2b reflects thermodynamic equilibrium between the transition metal and WS_2 such that no new phases are favored to form when the transition metal and WS_2 are placed in contact. This type of phase diagram is observed in the late transition metals from groups 8–12 for M = Fe, Ru, Os, Co, Rh, Ni, Pd, Pt, Cu, Ag, Au, and Hg.

Finally, there are a few systems where insufficient information is available to accurately predict whether reaction between the metal and WS_2 is favored (M = Tc, Re, Ir, Zn, and Cd).

3.1. Metal-Sulfide Dominant Systems

Ti, Zr, V, Cr, Mn, Al, and Ga are favored to form thermodynamically stable sulfides at the expense of WS_2; thus, their M–W–S ternary diagrams are metal-sulfide dominant at room temperature. The asterisks behind Ti and V denote that our categorization of these two metals is made even though these M–S binary phase diagrams are not very well established.

*Titanium**

There is no intermetallic phase in the Ti–W binary system, and the solubility of W in Ti is quite low [36]. Murray et al. reviewed the Ti–S binary system and published a Ti–S binary phase diagram. However, due to complexity of the Ti–S system, some of the equilibrium relationships among various Ti–S phases are unknown, and further experimental studies are required to construct a complete phase diagram [37]. Eleven titanium sulfides are depicted on the Ti–S phase diagram reported by Murray [37], with many additional superlattice structures reported near 60 at.% S, which is a region of the binary phase diagram that is uncertain. There are no ternary Ti–W–S phases reported for this system. Due to the ambiguity of the Ti–S binary phase diagram as well as a lack of thermodynamic data for most of these phases, a ternary Ti–W–S phase diagram could not be accurately calculated. However, based on the limited thermodynamic data available for Ti_2S [18], TiS [17], $TiS_{1.5}$ [18], TiS_2 [17], and TiS_3 [18], if a Ti–W–S ternary phase diagram were to be calculated, the resulting diagram would be metal sulfide dominant.

Zirconium

The Zr–S binary phase diagram [38] shows three stoichiometric compounds and a wide single-phase region from 50–64 at.% S denoted as $Zr_{1-x}S$. In this study, the published thermodynamic values for Zr_3S_4 (57 at.% S) [18] were used in our calculations in place of the values for $Zr_{1-x}S$ when estimating the ternary phase diagram. The thermochemistry of Zr_3S_2 has not been very well studied, and while Mompean et al. included an estimate of its enthalpy and entropy of formation [39], they excluded those numbers from their more conclusive table of values for all the Zr–S phases. One Zr–W intermetallic phase exists

[40], but there is no known Zr–W–S ternary phase. As shown in Figure 3a, when excess Zr reacts to completion with WS_2, it will consume WS_2 to form Zr_3S_2 and ZrW_2. In the case of excess WS_2, W and ZrS_2 are predicted to form at equilibrium.

*Vanadium**

V and W form a miscible solid solution at all temperatures [41]. Smith et al. reviewed the V–S system [42]. Their assessed V–S phase diagram is tentative due to difficulties in determining the equilibrium phases. Six vanadium sulfides are included in the binary phase diagram: VS_4, VS, V_3S_4, V_5S_8, V_5S_4, and V_3S [42]. Some other V–S phases such as V_2S_5, VS_3, and VS_5 have also been reported, but are disputed in the literature [42]. No V–W–S ternary phase has been reported. Due to a lack of thermodynamic data for most V–S phases, a conclusive calculation could not be made. When we calculated the diagram using three V–S phases for which data are more certain (VS, V_2S_3, and VS_4), the V–W–S ternary phase diagram was predicted to be metal sulfide dominant.

Chromium

Cr and W are immiscible and do not form any binary Cr–W phases [43]. Several intermediate Cr–S phases have been reported, all with compositions from 50–60 at.% S [44]. However, there is disagreement about the exact list of stable compounds. Waldner et al. conducted a thorough review of this binary system and presented thermodynamic values that are internally consistent [45], so this study adopted their results to calculate the Cr–W–S ternary phase diagram. The resulting diagram, seen in Figure 3b, is dominated by those stable Cr–S binary phases. However, based on our thermodynamic data and calculation, we could not confidently determine whether many of the Cr–S phases would be in equilibrium with W or WS_2 because the absolute values of ΔG°_{rxn} for those reactions are smaller than our benchmark value of 8 kJ/(mol of atoms).

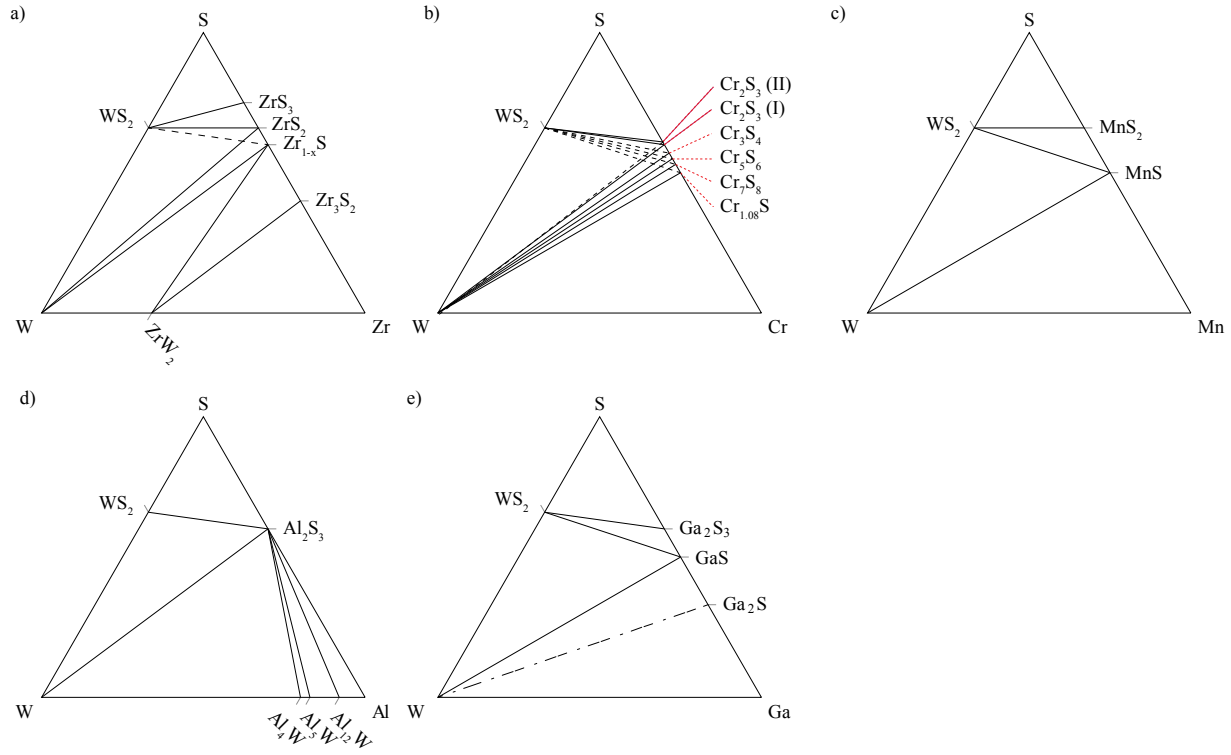

Fig 3. Calculated M–S dominant phase diagrams at 298 K for the (a) Zr–, (b) Cr–, (c) Mn–, (d) Al–, and (e) Ga–W–S ternary systems. Dashed lines in (a) and (b) indicate tie lines that are unstable by a narrow margin, and the dot-dash line in (e) indicates a binary phase which may not be stable.

Manganese

Calculation of the Mn–W–S ternary phase diagram relies on data for the Mn–S binary system discussed by Domask et al. [16]. There are only two room-temperature Mn–S phases and no Mn–W phase [46,47]. The thermodynamic data of the Mn–S phases were obtained from [17,48]. The resulting ternary phase diagram is dominated by the Mn–S phases, as shown in Figure 3c.

Aluminum

There is only one Al–S phase (Al_2S_3) in the Al–S binary phase diagram [49]. Several Al–W phases were reported in that binary phase diagram [50]. There is no ternary phase diagram in the Al–W–S system nor any known ternary Al–W–S phases. The calculated ternary phase diagram is shown in Figure 3d, which is dominated by the stable Al_2S_3 phase.

Gallium

There is no Ga–W binary phase diagram, but an absence of atmospheric-pressure binary phases is reported, and there is limited solubility [51]. As many as four Ga–S room-temperature phases have been included in the Ga–S binary phase diagram (Ga_2S, GaS, Ga_4S_5, and GaS_2), but only two (GaS and GaS_2) are consistently included [52–55]. Work by Pardo et al. exploring that system between 50 and 66 at.% S culminated in the publication of a Ga–S phase diagram [54], showing that Ga_4S_5 is not stable below 1131 K; therefore, we excluded it from our room-temperature diagram. Little work has been done to confirm the room-temperature stability of Ga_2S, so it is included it in the diagram, but the tie-line to it is dot-dashed to indicate this uncertainty. The thermodynamic data for the gallium sulfides is from Moiseev and Šesták [56]. The resulting Ga–S–W phase diagram, Figure 3e, shows WS_2 reacting with Ga to form binary gallium sulfides and W.

3.2. Ternary Phase/Solid Solution Dominant Systems

A ternary phase or solid solution is important in a number of early transition metal systems: the Hf–, Nb–, Ta–, Mo–W–S ternary systems, as well as in the In–W–S system.

Hafnium

In the binary Hf–W system, one intermetallic phase, HfW_2 was reported in [57]. A binary Hf–S phase diagram is not available, but the Hf–S binary phases were discussed in [16]. A ternary phase, Hf_9W_4S, was reported in [25,35]. The structure of this phase has Hf and W distributed in an ordered manner, forming the host lattice, while S occupies the interstices [35]. A ternary phase diagram could not be calculated due to lack of thermodynamic data for Hf_9W_4S. However, the ternary phase diagram is metal-sulfide dominant if we consider only the phase equilibria of the well-studied stable phases HfW_2 [19], HfS_2 [58] and HfS_3 [58].

Niobium and Tantalum

Both Nb and Ta form miscible solid solutions with W [59,60]. Several Nb–S binary phases are reported in the literature [61]. A Ta–S binary phase diagram is currently not available. Due to the similarities between Nb, Ta, and W, atoms of either Nb or Ta can replace some of the W atoms in WS_2. NbS_2 and TaS_2 also have a layered crystal structure similar to the prototypical 2H-MoS_2 structure seen in WS_2, but that structure is not the most thermodynamically stable structure of either NbS_2 or TaS_2 at room temperature [27,62]. Therefore, Golubnichaya et al. experimentally investigated the NbS_2–WS_2 and TaS_2–WS_2 systems to determine the mutual solubility of WS_2, NbS_2 and TaS_2. They observed that there was considerable solubility of WS_2 in NbS_2 (~25 at.% WS_2) and of NbS_2 in WS_2 (~22.5 at.% NbS_2) [27]. Solubility of WS_2 in TaS_2 was more limited, but a large amount of TaS_2 could be dissolved in WS_2 (~75 at.% TaS_2). Other than these solid solutions, the intermediate ternary phase Nb_3WS_8 is also reported [26]. Due to lack of information about thermodynamic data for these two systems, ternary phase diagrams were not calculated in this study.

Molybdenum

The Mo–W binary phase diagram [63] shows complete miscibility between Mo and W. A ternary phase diagram, published by Moh et al. [34], shows complete solid solubility between MoS_2 and WS_2 [34,64], as redrawn in Figure 4. The two solution phases are in equilibrium with each other. However, Mo and WS_2 are favored to form MoS_2 and W metal. When there is excess Mo, the W in the WS_2 lattice will be replaced by Mo, and the excess Mo will form a solid solution with the liberated W at thermodynamic equilibrium. In the opposite case, when there is excess WS_2 in the system, the Mo will substitute for W, leading to a $W_xMo_{1-x}S_2$ solid solution that is as rich as possible in MoS_2. In general, WS_2 would be consumed upon reaction with Mo to lower the free energy of the system.

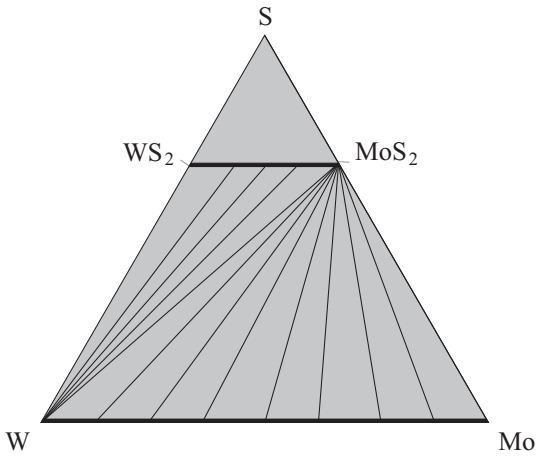

Fig 4. Mo–W–S phase diagram at 773 K, adapted from Moh et al. [34]**. Bold lines are single-phase solid solution regions, and grey areas are two-phase regions. Tie lines in the bottom half of the diagram do not divide adjacent phase fields, but instead indicate the compositions of the two solid solutions in equilibrium with each other.**

Indium

There is a lack of consensus about the In–S binary system: there is no agreement on the equilibrium In-rich phases, nor any investigation above 60 at.% S [65]. Also, there is no In–W phase diagram, although no intermediate phases and low solubility have been reported [66]. Therefore, no ternary phase diagram could be calculated. Of note, In forms an intercalation compound with WS_2 (In_xWS_2, where $0 \leq x \leq 1$) where the In likely has trigonal prismatic coordination [28].

3.3. WS_2 Dominant Systems

Per our calculations, Fe, Ru, Os, Co, Rh, Ni, Pd, Pt, Cu, Ag, Au, and Hg are all predicted to be in thermodynamic equilibrium with WS_2 at 298K. Therefore, their ternary phase diagrams are WS_2 dominant. The M–S thermodynamic data for the Fe, Ru, Os, Rh, Pd, Pt, Cu, and Au–S systems were tabulated and discussed in our earlier paper [16], and are adopted in this study; therefore, our current study focuses on the M–W intermetallic phases, the M–S systems not addressed in our earlier study. and the resulting M–W–S ternary phase diagrams.

Iron

Multiple papers describe the Fe–W–S ternary system at high temperature [20,22,67]. Štemprok et al. published a high-temperature Fe–W–S ternary phase diagram for temperature near but below 1016 K, as redrawn in Figure 5a. This phase diagram is iron sulfide dominant, which means that iron has a stronger affinity for sulfur than tungsten [67]. They annealed Fe and WS_2 at 947 K for 825 h, and produced W, WS_2, and $Fe_{1-x}S$. The position of the W–$Fe_{1-x}S$ tie line was also confirmed by several "appearance of phase" experiments [22]. Ternary phases in the Fe–W–S system have not been reported to date.

Our study calculated the Fe–W–S ternary phase diagrams at 298 K. We used both the Fe–S binary phase diagram and the thermodynamic data from [68] because the paper is thorough and internally consistent. On the other hand, binary phases in the Fe–W binary system are not well agreed upon [22,67,69–71]. The free energy of formation of these binary phases at 298 K, where reported from experiments [72,73], is close to zero. Miedema's prediction [19] also places the enthalpy of formation at 298 K at zero. A more recent study shows that Fe_2W is a metastable transitional phase [71]. Furthermore, there is some speculation that Fe–W binary phases in earlier reports may have been stabilized by carbon impurities [74]. Therefore, in this study, we included only FeW near 50 at.% W, following Naidu et al. [70]. We adopted the enthalpy and entropy of formation of the FeW phase reported for the Fe_7W_6 phase [19] due to the similarity in composition. In our ternary phase diagram at 298 K, the tie-line to this phase is shown with a dot-dash line to reflect this uncertainty.

The calculated ternary phase diagram at room temperature is WS_2 dominant, as shown in Figure 5b. Due to a lack of thermodynamic data, we did not calculate a high temperature Fe–W–S ternary phase diagram. It is hard to compare our calculation performed for 298 K with the high-temperature diagram since there are many differences in the binary phases in the Fe–S system at these two temperatures.

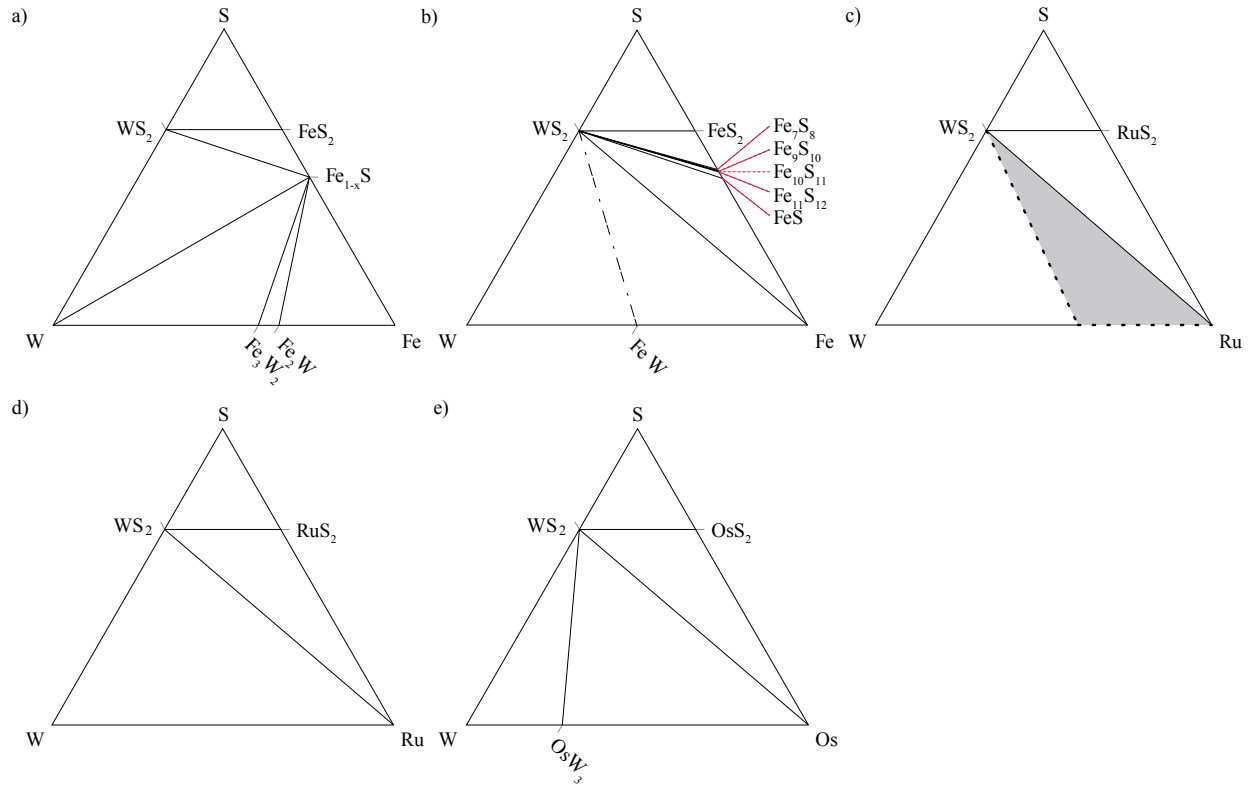

Fig 5. Group 8: The Fe–W–S system: (a) High temperature phase diagram near but below 1016 K, adapted from Štemprok [22] and (b) calculated phase diagram at 298 K. The dot-dash line reflects our own uncertainty about whether FeW is truly an equilibrium phase in the binary system. The Ru–W–S system: (c) A W solubility up to 40 at.% (solubility at 1773 K) was incorporated into the calculation, and the Ru–W solid solution was found to be in equilibrium with WS_2, which is indicated by the shaded region. The dotted lines mean the actual solubility of W in Ru at room temperature is uncertain. (d) A simplified Ru–W–S ternary phase diagram at 298 K in which W solubility in Ru is not indicated. (e) The Os–W–S ternary phase diagram calculated at 298 K. All of these systems (except (a) Fe–W–S at high temperature) have WS_2 dominant ternary phase diagrams.

Ruthenium

The Ru–W–S ternary phase diagram in Figure 5c was drawn relying on the corresponding binary phase diagrams from [75,76]. No intermetallic phase was found in the Ru–W system, but the solid solubility of W in Ru is very high regardless of the crystal structural differences between hexagonally close-packed Ru and body-centered cubic W [75]. We incorporated 40 at.% W solubility in Ru (solubility at 1773 K [75]) into our calculation as discussed in Section 2.2. The resulting phase diagram at 298 K was

WS_2 dominant, as shown in Figure 5c. However, considering the inclusion of solubility did not alter any of the phases in equilibrium with each other, we decided not to depict this solubility for any of the other systems with significant solubility for simplification. A simplified Ru–W–S ternary phase diagram is shown in Figure 5d, which is the style we adopt in the rest of the paper.

Osmium

The Os–W–S ternary system is similar to the Ru–W–S ternary system, except there is one intermetallic phase in the Os–W binary system [77]. We denoted this phase, from 64 to 78 at.% W, as OsW_3 in our calculation [77]. Os is also hexagonally close-packed, but the solubility of W in Os is rather high. We included 30 at.% W solubility in Os (solubility at 1273 K [77]) in our calculation, but it did not change which phases were in equilibrium with each other. The calculated ternary phase diagram at 298 K, based on the corresponding binary phase diagrams [77,78], is WS_2 dominant, as shown in Figure 5e.

Cobalt

In the Co–W–S system, there are two Co–W intermetallic phases (Co_7W_6, Co_3W) [79] and three Co–S phases (CoS_2, Co_3S_4, Co_9S_8) [80] stable at room temperature. No ternary phase was found for this system. The calculated ternary phase diagram is WS_2 dominant, as shown in Figure 6a, but it would have mixed dominance if the narrowly unstable dashed tie-lines were actually stable.

Rhodium

For the Rh–W–S system, Rh_2S_3 [17], Rh_3S_4 [17], and $Rh_{17}S_{15}$ [81] were selected as the Rh–S binary phases in this study [82], and RhS_2 was excluded as in [16]. For the Rh–W phases, one intermetallic phase from 21 to 42 at.% W [83] exists in this system at 1473 K. In our study, we assumed this phase is stable at room temperature, and treated it as the line compound Rh_7W_3. The regular solution model was also applied due to the high solubility of W in Rh. Up to 15 at.% W solubility in Rh (solubility at 1473 K [83]) was incorporated into the calculation using the approach from Section 2.2. The resulting ternary phase diagram remained the same type as the one we calculated without considering the solid

solution. It is WS_2 dominant, as shown in Figure 6b, but it could alternatively have mixed dominance if the narrowly unstable dashed tie-lines are actually stable.

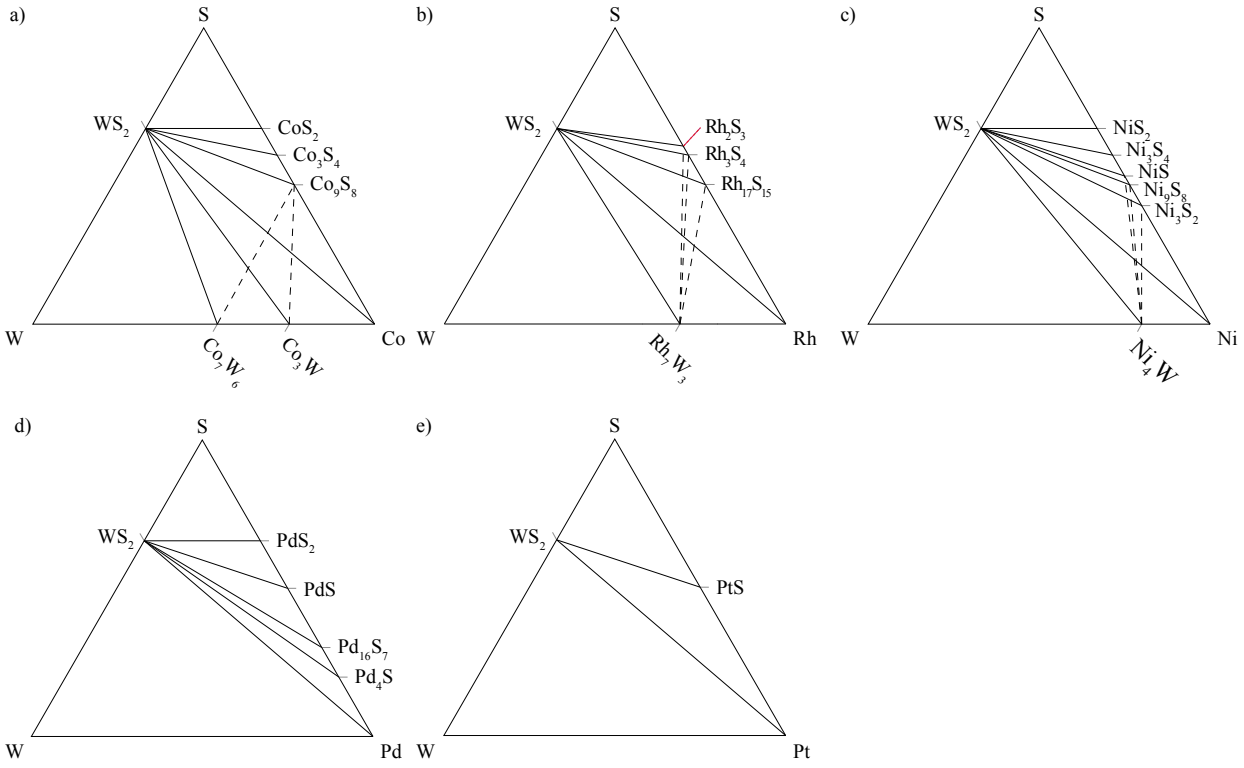

Fig 6. Groups 9 and 10: Calculated ternary phase diagrams at 298 K in the (a) Co–, (b) Rh–, (c) Ni–, (d) Pd–, and (e) Pt–W–S systems. Dashed lines indicate tie lines that are unstable by a narrow margin. All of the ternary phase diagrams are WS_2 dominant.

Nickel

Naidu et al. conducted a review of the Ni–W binary system [84]. Their final binary phase diagram shows three stable, room-temperature intermetallic compounds: Ni_4W, NiW and NiW_2. However, a recent paper [74] refuted the existence of the NiW and NiW_2 phases on the basis of new experiments. Both NiW and NiW_2 were not detected in very carefully controlled arc-melted samples. On the other hand, after generating samples using a traditional thin-film diffusion couple, the authors reproduced the X-ray diffraction patterns for NiW and NiW_2 seen in prior work, but detected carbon contamination. Their study concluded that what had been previously described as NiW was in fact the ternary carbide Ni_6W_6C, and what was previously described as NiW_2 was, similarly, Ni_2W_4C. They concluded that Ni_4W is the only

room-temperature intermetallic phase in the Ni–W binary system, and this finding is reflected in our study. (Additionally, when these two questionable phases—NiW and NiW_2 [19]—were included in our calculation, the overall structure of the resulting ternary phase diagram did not change. It remained WS_2 dominant.)

The Ni–S system over the full composition range was investigated by [85]. Stølen further considered the range 44–48 at.% S [86] and concluded that Ni_9S_8 and not Ni_7S_6 is the stable phase at room temperature. The estimated data in Waldner et al. [87] was used to calculate Figure 6c. There is no Ni–W–S ternary phase reported in the literature. Ni–W–S ternary phase diagram is WS_2 dominant, as shown in Figure 6c, even when narrowly unstable tie-lines are considered.

Palladium

Figure 6d shows the ternary phase diagram of the Pd–W–S system, which is WS_2 dominant at room temperature. The calculations were based on thermodynamic data of Pd–S phases from [17,88]. No M–W intermetallic phases were found, but large solubility of W was observed in the Pd–W binary phase diagram [89]. Pd has the face-centered cubic crystal structure, and W has the body-centered cubic crystal structure [89]. The Pd–W solid solution was treated as discussed in Section 2.2. Our calculation incorporated up to 22 at.% W solubility in Pd (solubility at 1273 K [89]). No tie-line was altered when taking the W solubility into consideration.

Platinum

Knapton et al. [90] reported Pt_3W and Pt_3W_2 phases that are analogous to the Pt_3Mo and Pt_3Mo_2 phases at 1673 K, and Sinha et al. [91] reported the existence of Pt_2W phase with an orthorhombic Pt_2Mo type structure at 1173 K, but none of these intermetallic phases were confirmed at room temperature. In fact, the thermodynamic stability of these intermetallic phases has been disputed in the literature [90–94]. Therefore, the Pt–W–S ternary phase diagram, as shown in Figure 6e, was drawn based only on the thermodynamic data of Pt–S phases from [17]. However, even if we include the Pt–W intermetallic

phases in the calculation using thermodynamic data from Miedema's estimation [19], the ternary diagram remains WS_2 dominant at room temperature. In addition, despite the crystal structure differences between face-centered cubic Pt and body-centered cubic W, up to 60 at.% W solubility in Pt was shown in the Pt–W binary phase diagram [94], which was incorporated into the ternary phase diagram calculation as discussed in Section 2.2. The ternary phase diagram type did not change compared to a calculation neglecting solid solubility.

Copper

The Cu–W–S system has been studied by Moh et al. from near room temperature up to 1173 K [64]. In their study, no ternary Cu–W–S compounds were found. Therefore, the phases shown in the ternary phase diagram are limited to elemental and binary phases [95,96]. A ternary phase, $Cu_{12}S_{59}W_{29}$, is reported in [29], but it is described as a metastable solid solution of Cu in WS_2. The original research [30] found that o-WS_2, obtained by electrochemical oxidation of $Na_x(H_2O)_y[WS_2]$, could undergo intercalation reactions to accommodate a large variety of guest species, including metals with low ionization energy, e.g., Cu or Ag. However, this o-WS_2 was believed to be metastable and readily decomposes at temperatures greater than 403 K.

Moh et al. published a Cu–W–S ternary phase diagram at 973 K, as shown in Figure 7a. It is M–S dominant due to the considerably lower affinity of W for S compared to Cu for S. However, due to the decomposition of the dominant Cu_2S phase below 348 K, as discussed in [16,96], the room-temperature Cu–W–S ternary phase diagram cannot be the same as that at 973 K. The thermodynamic data of the room-temperature Cu–S binary phases were obtained from [97]. The calculated room-temperature diagram, Figure 7b, is WS_2 dominant. We also calculated the Cu–W–S ternary phase diagram at 950 K based on thermodynamic data for the $Cu_{2-x}S$ phase from [98], WS_2 phase from [20], and the pure elements from [19]. Our results agreed with the published ternary phase diagram by Moh et al. in Figure 7a.

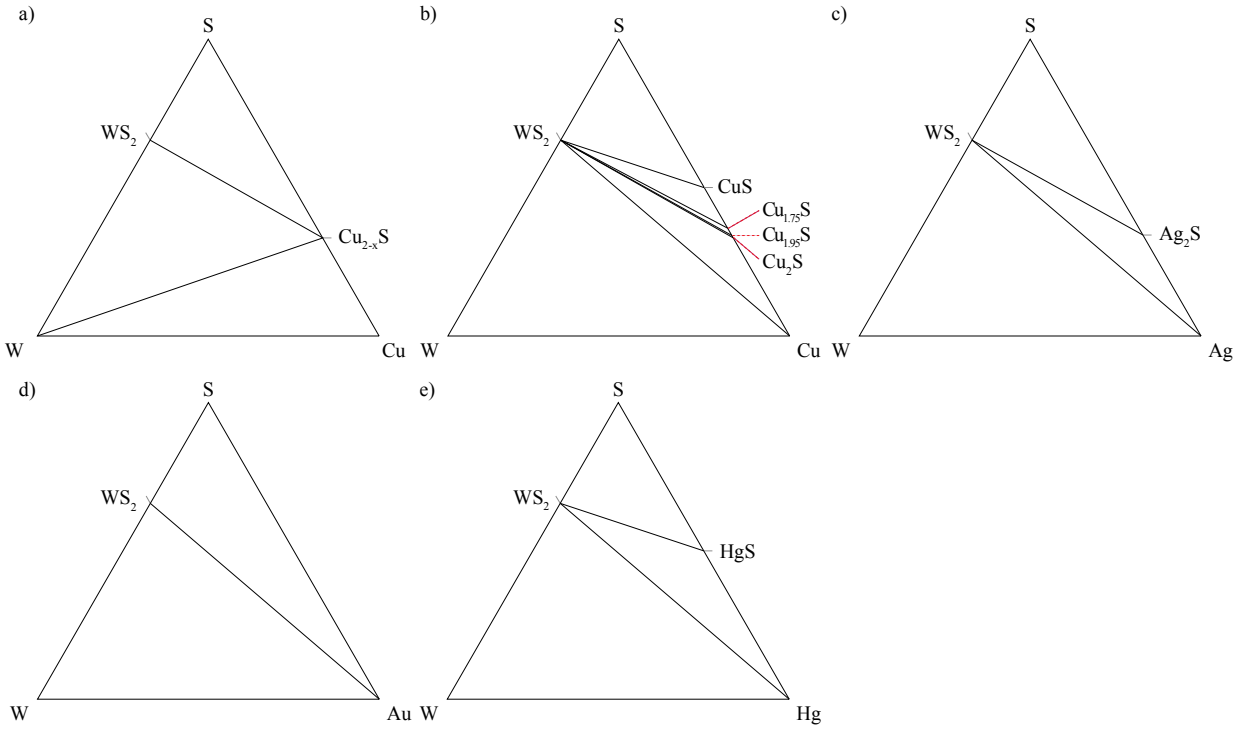

Fig 7. Groups 11 and 12: (a) Cu–W–S phase diagram at 973 K, adapted from Moh et al. [64] **and calculated phase diagrams for the (b) Cu–, (c) Ag–, (d) Au–, and (e) Hg–W–S systems at 298 K.**

Silver and Gold

Ag–W, Au–W, and Au–S show complete immiscibility at room temperature [99–101]. The Ag–S system has only one binary phase, Ag_2S, at room temperature. A ternary phase, $Ag_{12}S_{59}W_{29}$, is described in the literature as intercalation of Ag into o-WS_2 [30], but the researchers concluded that the phase is metastable. The estimated ternary phase diagrams for the Ag–W–S and Au–W–S systems are shown in Figure 7c and Figure 7d, and are both WS_2 dominant.

Mercury

A binary Hg–S phase diagram shows one binary phase, HgS, which has three atmospheric pressure structures before melting at 1093 K [102]. No Hg–W phase diagram exists, but no intermetallic phases have been found and there is limited solubility [103]. In addition, Miedema predicted such high (positive) enthalpy of formation for Hg–W phases that intermetallic phases are unlikely to exist. Figure 7e shows the calculated Hg–W–S ternary phase diagram, dominated by WS_2. Although liquid Hg beads

might serve as a convenient temporary contact for materials characterization in a properly designed laboratory set-up, its high vapor pressure and toxicity, along with its melting point below room temperature, make it unsuitable as a contact for most device applications.

3.4. Other M–W–S systems

In the last few systems (M = Tc, Re, Ir, Zn, and Cd), there is insufficient information to calculate a ternary phase diagram, but all available information is discussed below.

Technetium, Rhenium, Iridium, Zinc, and Cadmium

For three of these systems (M = Tc, Re, and Ir), M–W binary phase diagrams are available, but the M–S binary phase diagrams are not available [21]. For the other two systems (M = Zn and Cd), the M–S diagrams are published, but the M–W binary phase diagrams are not [21]. For most of the binary phases in these systems, there is limited thermodynamic data available. Therefore, we were not able to calculate M–W–S ternary phase diagrams for the Tc–, Re–, Ir–, Zn–, and Cd–W–S systems.

3.5. Comparison between the M–W–S and M–Mo–S systems

WS_2 and MoS_2 have a similar layered structure with lattice parameters that differ by less than 0.2% in the *a*-direction and less than 0.6% in the *c*-direction [1,16]. Monolayer WS_2 has a bandgap of 2.05 eV, while the bandgap of monolayer MoS_2 is 1.89 eV [10]. The Gibbs free energy of formation of WS_2 at room temperature is −83.3 kJ/(mol of atoms), and for MoS_2, it is −88.9 kJ/(mol of atoms) [18]. These similarities result in similar interactions with many transition metals. Many of the early transition metals (groups 4 to 7) either react with WS_2 and MoS_2 to form metal sulfides, create solid solutions by substituting for W/Mo, or form ternary phases. Their phase diagram type is often metal sulfide dominant or ternary/solid solution dominant. Transition metals from group 8 to group 11 are generally in

equilibrium with WS_2 and MoS_2, except for systems where ternary phases exist. Figure 8a shows a periodic table depicting the ternary phase diagram types of the M–Mo–S systems, and Figure 8b shows a similar periodic table for the M–W–S systems from groups 4 through 11 to match the earlier work. Lastly, there are many more ternary phases in the M–Mo–S systems than in the M–W–S systems due to the lack of stable W analogues of the ubiquitous M–Mo–S Chevrel phases [31].

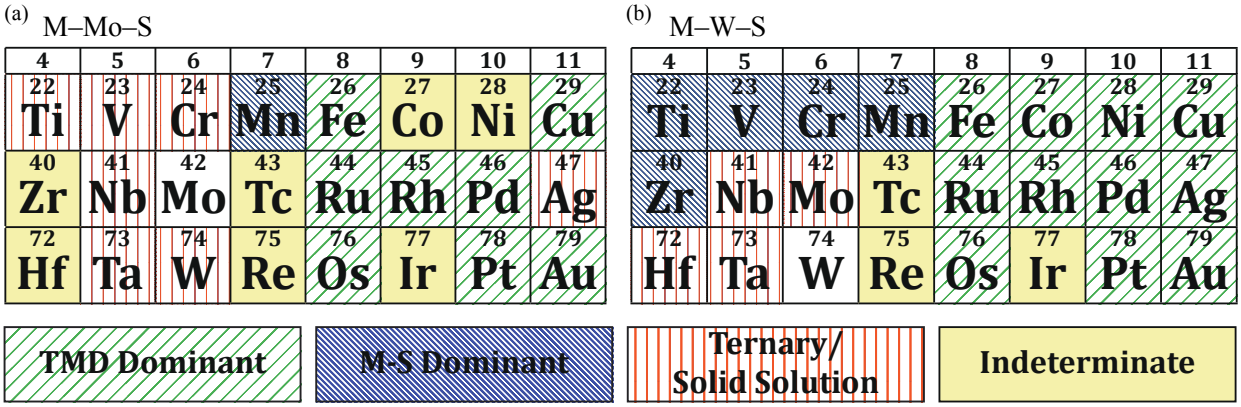

Fig 8. (a) Periodic table depicting ternary phase diagram types of M–Mo–S systems, adapted from Domask et al. [16]**. (b) Periodic table showing ternary phase diagram types of M–W–S systems (groups 4 to 11 only to match the earlier work). Rather than MoS_2 or WS_2 dominant, we refer to such systems as transition metal dichalcogenide (TMD) dominant.**

4. Conclusions

In summary, we studied the interactions between metals and WS_2, and calculated 17 M–W–S ternary phase diagrams at room temperature. We observed that the early transition metals from group 4 to group 7, as well as group 13, are either favored to react with WS_2 to create binary or ternary phases, or to form solid solutions by substituting for W. For M = Zr, Cr, Mn, Al, and Ga, the calculated M–W–S ternary phase diagrams are metal sulfide dominant. Additionally, by omitting certain phases and information, we were also able to predict Hf–, Ti–, and V–W–S ternary phase diagrams to be metal-sulfide dominant. In each of these cases, the metal forms a very stable sulfide at the expense of WS_2. Most of the late transition metals, from group 8 to group 12, are in thermodynamic equilibrium with WS_2,

and are not predicted to react with the metals to form any new phases. For M = Fe, Ru, Os, Co, Rh, Ni, Pd, Pt, Cu, Ag, Au, and Hg, the calculated M–W–S ternary phase diagrams are WS_2 dominant at room temperature. In a few systems, our calculations were limited because ternary phases exist without available thermodynamic data (M = Hf, Nb, and In); important binary phase diagrams are not available (M = Hf, Ta, Tc, Re, Ir, Zn, Cd, and In); or the binary phase diagrams are not well agreed upon (M = Ti and V). The many M–W–S calculated ternary phase diagrams presented here give researchers insights into potential reactions between contact metals and WS_2 for future studies.

5. Acknowledgements

The authors would like to thank the National Science Foundation (DMR 1410334) for their support of this project.

6. References

[1] W. Jaegermann, H. Tributsch, Prog. Surf. Sci. 29 (1988) 1–167.

[2] R. Levi, O. Bitton, G. Leitus, R. Tenne, E. Joselevich, Nano Lett. 13 (2013) 3736–3741.

[3] H.E. Sliney, Tribol. Int. 15 (1982) 303–315.

[4] C.F. Higgs, C.A. Heshmat, H. Heshmat, J. Tribol. 121 (1999) 625–630.

[5] D. Voiry, H. Yamaguchi, J. Li, R. Silva, D.C.B. Alves, T. Fujita, M. Chen, T. Asefa, V.B. Shenoy, G. Eda, M. Chhowalla, Nat. Mater. 12 (2013) 850–855.

[6] G. Alonso, M. Del Valle, J. Cruz, A. Licea-Claverie, V. Petranovskii, S. Fuentes, Catal. Lett. 52 (1998) 55–61.

[7] S.Z. Butler, S.M. Hollen, L. Cao, Y. Cui, J.A. Gupta, H.R. Gutiérrez, T.F. Heinz, S.S. Hong, J. Huang, A.F. Ismach, E. Johnston-Halperin, M. Kuno, V. V Plashnitsa, R.D. Robinson, R.S. Ruoff, S. Salahuddin, J. Shan, L. Shi, M.G. Spencer, M. Terrones, W. Windl, J.E. Goldberger, ACS Nano 7 (2013) 2898–2926.

[8] S. Das, J.A. Robinson, M. Dubey, H. Terrones, M. Terrones, Annu. Rev. Mater. Res. 45 (2015) 1–27.

[9] S. Das, M. Kim, J. Lee, W. Choi, Crit. Rev. Solid State Mater. Sci. 39 (2014) 231–252.

[10] A. Kumar, P.K. Ahluwalia, Eur. Phys. J. B 85 (2012) 18–22.

[11] H.R. Gutiérrez, N. Perea-López, A.L. Elías, A. Berkdemir, B. Wang, R. Lv, F. López-Urías, V.H. Crespi, H. Terrones, M. Terrones, Nano Lett. 13 (2012) 3447–3454.

[12] W. Zhao, Z. Ghorannevis, L. Chu, M. Toh, C. Kloc, P.-H. Tan, G. Eda, ACS Nano 7 (2012) 791–797.

[13] L. Liu, S.B. Kumar, Y. Ouyang, J. Guo, IEEE Trans. Electron Devices 58 (2011) 3042–3047.

[14] W.S. Hwang, M. Remskar, R. Yan, V. Protasenko, K. Tahy, S.D. Chae, H. Xing, A. Seabaugh, D. Jena, Appl. Phys. Lett. 101 (2012) 013107.

[15] M. Etman, M. Neumann-Spallart, J. Electroanal. Chem. Interfacial Electrochem. 269 (1989) 411–422.

[16] A.C. Domask, R.L. Gurunathan, S.E. Mohney, J. Electron. Mater. 44 (2015) 7–9.

[17] O. Kubaschewski, C.B. Alcock, P.J. Spencer, Materials Thermochemistry, Pergamon Press, New York, 1993.

[18] K.C. Mills, Thermodynamic Data for Inorganic Sulphides, Selenides and Tellurides, Butterworths, London, 1974.

[19] F.R. de Boer, W.C.M. Mattens, R. Boom, A.R. Miedema, A.K. Niessen, Cohesion in Metals, North-Holland, Amsterdam, 1988.

[20] R. Vogel, H. Weizenkorn, Arch. Eisenhüttenwes. 32 (1961) 413–420.

[21] T.B. Massalski, H. Okamoto, P.R. Subramanian, L. Kacprzak, W.W. Scott (Eds.), Binary Alloy Phase Diagrams, vol. 1–3, ASM International, Materials Park, OH, 1990.

[22] M. Štemprok, Miner. Depos. 6 (1971) 302–312.

[23] J. Wildervanck, F. Jellinek, Z. Anorg. Allg. Chem. 328 (1964) 309–318.

[24] R. Voorhoeve, H. Wolters, Z. Anorg. Allg. Chem. 376 (1970) 165–179.

[25] A. Harsta, E. Wennebo, Acta Chem. Scand. A 35A (1981) 227–230.

[26] V.L. Kalikhman, A.A. Golubnichaya, Kristallografiya 28 (1983) 801– 802.

[27] A.A. Golubntchaya, V.L. Kalikhman, Inorg. Mater. Transl. from Izv. Akad. Nauk Sssr, Neorg.

Mater. 10 (1974) 1018–1020.

[28] S.K. Srivastava, B.N. Avasthi, Synth. Met. 10 (1985) 213–221.

[29] P. Villars, A. Prince, H. Okamoto (Eds.), Handbook of Ternary Alloy Phase Diagrams, vol. 1–10, ASM International, Materials Park, OH, 1995.

[30] R. Schöllhorn, U. Bethel, W. Paulus, Rev. Chim. Minér. 21 (1984) 545–555.

[31] R. McCarley, S. Hilsenbeck, X. Xie, J. Solid State Chem. 117 (1995) 269–274.

[32] W.E. Liu, S.E. Mohney, Mater. Sci. Eng. B-Solid 103 (2003) 189–201.

[33] W.E. Liu, S.E. Mohney, J. Electron. Mater. 32 (2003) 1090–1099.

[34] G. Moh, G. Udubasa, Chem. Erde 35 (1976) 327–335.

[35] A. Harsta, S. Rundqvist, J. Solid State Chem. 70 (1987) 210–218.

[36] J.L. Murray, in: T.B. Massalski (Ed.), Binary Alloy Phase Diagrams, Chap. Ti–W (Titanium–Tungsten), vol. 3, second ed., ASM International, Materials Park, OH, 1990, pp. 3494–3497.

[37] J.L. Murray, Bull. Alloy Phase Diagr. 7 (1986) 156–163.

[38] H. Okamoto, in: T.B. Massalski (Ed.), Binary Alloy Phase Diagrams, Chap. S–Zr (Sulfur–Zirconium), vol. 3, second ed., ASM International, Materials Park, OH, 1990, pp. 3300–3301.

[39] F. Mompean, J. Perrone, M. Illemassène, Chemical Thermodynamics of Zirconium, vol. 8, Elsevier, Amsterdam, 2005.

[40] S.V.N. Naidu, A.M. Sriramamurthy, P.R. Rao, J. Alloy Phase Diagr. 3 (1987) 47–56.

[41] S.V.N. Naidu, A.M. Sriramamurthy, P.R. Rao, in: T.B. Massalski (Ed.), Binary Alloy Phase Diagrams, Chap. V–W (Vanadium–Tungsten), vol. 3, second ed., ASM International, Materials Park, OH, 1990, pp. 3523–3524.

[42] J.F. Smith, in: T.B. Massalski (Ed.), Binary Alloy Phase Diagrams, Chap. S–V (Sulfur–Vanadium), vol. 3, second ed., ASM International, Materials Park, OH, 1990, pp. 3292–3295.

[43] S.V.N. Naidu, A.M. Sriramamurthy, P.R. Rao, T. Indian Inst. Met. 36 (1983) 24–29.

[44] M. Venkatraman, J.P. Neumann, in: T.B. Massalski (Ed.), Binary Alloy Phase Diagrams, Chap. Cr–S (Chromium–Sulfur), vol. 2, second ed., ASM International, Materials Park, OH, (1990) pp. (1990) 1322–1326.

[45] P. Waldner, W. Sitte, Int. J. Mater. Res. 102 (2011) 1216–1225.

[46] H.F. Franzen, in: T.B. Massalski (Ed.), Binary Alloy Phase Diagrams, Chap. Mn–S (Manganese–Sulfur), vol. 3, second ed., ASM International, Materials Park, OH, 1990, pp. 2593–2597.

[47] S.V.N. Naidu, P.R. Rao, in: T.B. Massalski (Ed.), Binary Alloy Phase Diagrams, Chap. Mn–W (Manganese–Tungsten), vol. 3, second ed., ASM International, Materials Park, OH, 1990, pp. 2623.

[48] D. Dilner, H. Mao, M. Selleby, Calphad 48 (2015) 95–105.

[49] R.C. Sharma, Y.A. Chang, in: T.B. Massalski (Ed.), Binary Alloy Phase Diagrams, Chap. Al–S (Aluminum–Sulfur), vol. 1, second ed., ASM International, Materials Park, OH, 1990, pp. 203–206.

[50] T.B. Massalski (Ed.), in: Binary Alloy Phase Diagrams, Chap. Al–W (Aluminum–Tungsten), vol. 1, second ed., ASM International, Materials Park, OH, 1990, pp. 234–235.

[51] S.V.N. Naidu, P.R. Rao, in: T.B. Massalski (Ed.), Binary Alloy Phase Diagrams, Chap. Ga–W (Gallium–Tungsten), vol. 2, second ed., ASM International, Materials Park, OH, 1990, pp. 1874.

[52] R.M.A. Lieth, H.J.M. Heijligers, C.W.M. vd Heijden, J. Electrochem. Soc. 113 (1966) 798–801.

[53] T.B. Massalski (Ed.), in: Binary Alloy Phase Diagrams, Chap. Ga–S (Gallium–Sulfur), vol. 2,

second ed., ASM International, Materials Park, OH, 1990, pp. 1849–1850.

[54] M.P. Pardo, M. Guittard, A. Chilouet, A. Tomas, J. Solid State Chem. 102 (1993) 423–433.

[55] A.Y. Zavrazhnov, D.N. Turchen, E.G. Goncharov, V.P. Zlomanov, J. Phase Equilib. 22 (2001) 482–490.

[56] G. Moiseev, J. Šesták, J. Therm. Anal. 43 (1995) 539–544.

[57] S.V.N. Naidu, A.M. Sriramamurthy, P.R. Rao, J. Alloy Phase Diagr. 3 (1987) 38–46.

[58] S. Fiechter, K. Eckert, J. Cryst. Growth 88 (1988) 435–441.

[59] S.V.N. Naidu, A.M. Sriramamurthy, P.R. Rao, J. Alloy Phase Diagr. 4 (1988) 184–190.

[60] R. Krishnan, S.P. Garg, N. Krishnamurthy, in: T.B. Massalski (Ed.), Binary Alloy Phase Diagrams, Chap. Ta–W (Tantalum–Tungsten), vol. 3, second ed., ASM International, Materials Park, OH, 1990, pp. 3438–3439.

[61] P.R. Subramanian, in: T.B. Massalski (Ed.), Binary Alloy Phase Diagrams, Chap. Nb–S (Niobium–Sulfur), vol. 3, second ed., ASM International, Materials Park, OH, 1990, pp. 2758–2762.

[62] C.J. Carmalt, T.D. Manning, I.P. Parkin, E.S. Peters, A.L. Hector, J. Mater. Chem. 14 (2004) 290.

[63] S.V.N. Naidu, A.M. Sriramamurthy, P.R. Rao, in: T.B. Massalski (Ed.), Binary Alloy Phase Diagrams, Chap. Mo–W (Molybdenum–Tungsten), vol. 3, second ed., ASM International, Materials Park, OH, 1990, pp. 2682–2686.

[64] G.H. Moh, in: F.L. Boschke (Ed.) Topics in Current Chemistry, vol. 76, Springer-Verlag, New York, 1978, pp. 107–151.

[65] H. Okomoto, in: T.B. Massalski (Ed.) Binary Alloy Phase Diagrams, Chap. In–S (Indium–Sulfur), vol. 3, second ed., ASM International, Materials Park, OH, 1990, pp. 2283–2285.

[66] S.V.N. Naidu, P.R. Rao in: T.B. Massalski (Ed.), Binary Alloy Phase Diagrams, Chap. In–W (Indium–Tungsten), vol. 3, second ed., ASM International, Materials Park, OH, 1990, pp. 2314.

[67] V. Raghavan, J. Alloy Phase Diagr. 4 (1988) 175–183.

[68] P. Waldner, A.D. Pelton, J. Phase Equilib. Diffus. 26 (2005) 23–38.

[69] J. Andersson, P. Gustafson, Calphad 7 (1983) 317–326.

[70] S.V.N. Naidu, A.M. Sriramamurthy, P.R. Rao, J. Alloy Phase Diagr. 2 (1986) 176–188.

[71] E.T. Henig, H. Hofmann, G. Petzow, in:, Die Konstitution von Fe–W–Ni Schwermetallegierungen und ihr Einfluss auf die Mechanischen Eigenschaften, Proc. l0th Plansee-Semin. 2, (1981) 335–359.

[72] T.N. Rezukhina, T.A. Kashina, J. Chem. Thermodyn. 8 (1976) 519.

[73] H. Kleykamp, J. Less-Common Met. 71 (1980) 127.

[74] R. Cury, J.M. Joubert, S. Tusseau-Nenez, E. Leroy, A. Allavena-Valette, S. Tusseaunenez, A. Allavena-Valette, Intermetallics 17 (2009) 174–178.

[75] E.J. Rapperport, M.F. Smith, Trans. Metall. Soc. AIME 230 (1964) 6–11.

[76] H. Okamoto, J. Phase Equilib. 12 (1991) 620.

[77] S.V.N. Naidu, A.M. Sriramamurthy, P.R. Rao, J. Alloy Phase Diagr. 2 (1986) 93–96.

[78] H. Okamoto, in: T.B. Massalski (Ed.) Binary Alloy Phase Diagrams, Chap. Os–S (Osmium–Sulfur), vol. 3, second ed., ASM International, Materials Park, OH, 1990, pp. 2949–2951.

[79] S.V.N. Naidu, A.M. Sriramamurthy, P.R. Rao, in: T.B. Massalski (Ed.) Binary Alloy Phase Diagrams, Chap. Co–W (Cobalt–Tungsten), vol. 2, second ed., ASM International, Materials Park, OH, 1990, pp. 1257–1259.

[80] Y.O. Chen, Y.A. Chang, Metall. Trans. B 9 (1978) 61–67.

[81] O. Diéguez, N. Marzari, Phys. Rev. B 80 (2009) 214115:1–6.

[82] H. Okamoto, in: T.B. Massalski (Ed.) Binary Alloy Phase Diagrams, Chap. Rh–S (Rhodium–Sulfur), vol. 3, second ed., ASM International, Materials Park, OH, 1990, pp. 3221–3224.

[83] S.V.N. Naidu, A.M. Sriramamurthy, P.R. Rao, J. Alloy Phase Diagr. 6 (1990) 137–141.

[84] S.V.N. Naidu, A.M. Sriramamurthy, P.R. Rao, in: T.B. Massalski (Ed.) Binary Alloy Phase Diagrams, Chap. Ni–W (Nickel–Tungsten), vol. 3, second ed., ASM International, Materials Park, OH, 1990, pp. 2882–2883.

[85] M. Singleton, P. Nash, K.J. Lee, in: T.B. Massalski (Ed.) Binary Alloy Phase Diagrams, Chap. Ni–S (Nickel–Sulfur), vol. 3, second ed., ASM International, Materials Park, OH, 1990, pp. 2850–2853.

[86] S. Stølen, H. Fjellvåg, F. Grønvold, H. Seim, E.F. Westrum, J. Chem. Thermodyn. 26 (1994) 987–1000.

[87] P. Waldner, A.D. Pelton, Z. Metallkd. 95 (2004) 672–681.

[88] A. Zubkov, T. Fujino, N. Sato, K. Yamada, J. Chem. Thermodyn. 30 (1998) 571–581.

[89] S.V.N. Naidu, A.M. Sriramamurthy, P.R. Rao, J. Alloy Phase Diagr. 6 (1990) 67–73.

[90] A.G. Knapton, Platin. Met. Rev. 24 (1980) 64–69.

[91] A.K. Sinha, Trans. Met. Soc. AIME. 245 (1969) 237–240.

[92] P. Greenfield, P.A. Beck, Trans. Met. Soc. AIME. 206 (1956) 265–276.

[93] A.G. Knapton, J. Inst. Met. 87 (1958) 28–32.

[94] S.V.N. Naidu, A.M. Sriramamurthy, P.R. Rao, J. Alloy Phase Diagr. 6 (1990) 74–79.

[95] P.R. Subramanian, D.E. Laughlin, in: T.B. Massalski (Ed.) Binary Alloy Phase Diagrams, Chap. Cu–W (Copper–Tungsten), vol. 2, second ed., ASM International, Materials Park, OH, 1990, pp. 1503–1504.

[96] D.J. Chakrabarti, D.E. Laughlin, Bull. Alloy Phase Diagr. 4 (1983) 254–271.

[97] R.W. Potter, Econ. Geol. 72 (1977) 1524–1542.

[98] F. Grønvold, E.F. Westrum, J. Chem. Thermodyn. 19 (1987) 1183–1198.

[99] S.V.N. Naidu, A.M. Sriramamurthy, P.R. Rao, J. Alloy Phase Diagr. 2 (1986) 210.

[100] H. Okamoto, T.B. Massalski, in: T.B. Massalski (Ed.) Binary Alloy Phase Diagrams, Chap. Au–W (Gold–Tungsten), vol. 1, second ed., ASM International, Materials Park, OH, 1990, pp. 451–453.

[101] R.C. Sharma, Y.A. Chang, in: T.B. Massalski (Ed.) Binary Alloy Phase Diagrams, Chap. Ag–S (Silver–Sulfur), vol. 1, second ed., ASM International, Materials Park, OH, 1990, pp. 86–87.

[102] R.C. Sharrna, Y.A. Chang, C. Guminski, J. Phase Equilib. 14 (1993) 101.

[103] S.V.N. Naidu, P.R. Rao, in: T.B. Massalski (ed.), Binary Alloy Phase Diagrams, Chap. Hg–W (Mercury–Tungsten), vol. 3, second ed., ASM International, Materials Park, OH, 1990, pp. 2180.

Appendix I

Table 1. Thermodynamic data used to calculate ternary phase diagrams at 298 K. Italicized ΔH_f° values indicate the use of Miedema's prediction as tabulated in de Boer [21]. Italicized ΔS_f° values indicate where the entropy was approximated as zero.

System	Phase	ΔH_f°	ΔS_f°	ΔG_f°	Ref
		kJ/(mol of atoms)	J/(K · mol of atoms)	kJ/(mol of atoms)	
W	WS_2	−86.47	−10.6	−83.3	[17]
Ti	Ti_2S	−93	2.3	−94	[18]
	TiS	−136.0	−3.1	−135.1	[17]
	$TiS_{1.5}$	−150	−6.38	−148	[18]
	TiS_2	−135.7	−5.50	−134.1	[17]
	TiS_3	−107.4	−8.98	−104.7	[18]
Zr	ZrW_2	*−12*	*0*	*−12*	[19]
	Zr_3S_2	−73.92	−5.14	−72.4	[39]
	Zr_3S_4	−203.8	−9.69	−200.9	[18]
	ZrS_2	−192.5	−8.26	−190.0	[18]
	ZrS_3	−157	−11.1	−154	[18]
V	VS	−96	−3.2	−95	[18]
	V_2S_3	−105	−5.62	−103	[18]
	VS_4	−60	−10.4	−57	[18]
Cr	$Cr_{1.03}S$	−76.54	2.1	−77.2	[45]
	Cr_7S_8	−83.43	0.2	−83.5	[45]
	Cr_5S_6	−85.47	−0.8	−85.2	[45]
	Cr_3S_4	−89.90	−2.16	−89.25	[45]
	Cr_2S_3(I)	−93.60	−5.06	−92.10	[45]
	Cr_2S_3(II)	−95.23	−7.67	−92.94	[45]
Mo	MoS_2	−91.9	−10.0	−88.9	[18]
Mn	MnS	−107.1	8.15	−110	[17]
	MnS_2	−74.6	1.303	−75.0	[48]

Fe	FeW	−0.4	*0*	−1	[19]
	FeS	−50.1	0.505	−50.2	[68]
	$Fe_{11}S_{12}$	−49.9	3.08	−50.8	[68]
	$Fe_{10}S_{11}$	−49.9	3.238	−50.9	[68]
	Fe_9S_{10}	−50.0	3.04	−51.0	[68]
	Fe_7S_8	−50.4	2.62	−51.1	[68]
	FeS_2	−57.0	−12.8	−53.2	[68]
Ru	RuS_2	−68.6	−12.7	−64.8	[17]
Os	OsW_3	*−9*	*0*	*−10*	[19]
	OsS_2	−49.0	−13.9	−44.8	[17]
Co	Co_3W	−2.0	1.2	−2.4	[19]
	Co_7W_6	−2.3	0.8	−2.5	[19]
	Co_9S_8	−50.1	−3.7	−49.0	[17]
	Co_3S_4	−51.28	−4.84	−49.84	[17]
	CoS_2	−51.03	−8.33	−48.55	[17]
Rh	Rh_7W_3	*−11*	*0*	*−11*	[19]
	$Rh_{17}S_{15}$	−44.4	*0*	−44.4	[81]
	Rh_3S_4	−51.1	−5.8	−49.4	[17]
	Rh_2S_3	−52.6	−6.7	−50.6	[17]
Ni	Ni_4W	−6.2	0.3	−6.3	[19]
	Ni_3S_2	−42.81	−3.64	−41.73	[87]
	Ni_9S_8	−45.31	−3.32	−44.31	[87]
	NiS	−46.31	−3.7	−45.2	[87]
	Ni_3S_4	−44.16	−3.69	−43.06	[87]
	NiS_2	−41.34	−4.04	−40.13	[87]
Pd	Pd_4S	−13.8	−0.6	−13.6	[17]
	$Pd_{16}S_7$	−25.22	*0*	−25.22	[88]
	PdS	−35.35	−6.7	−33.4	[17]
	PdS_2	−26.1	−4.7	−24.7	[17]

Pt	PtS	−41.6	−9.2	−38.9	[17]
Cu	Cu_2S	−26.81	5.735	−28.52	[97]
	$Cu_{1.95}S$	−27.06	4.98	−28.6	[97]
	$Cu_{1.75}S$	−27.64	3.07	−28.6	[97]
	CuS	−26.61	1.2	−27	[97]
Ag	Ag_2S	−10.6	8.77	−13.2	[17]
Hg	HgS	−26.7	−12.8	−22.9	[17]
Al	$Al_{12}W$	*−3.8*	*0*	*−3.8*	[19]
	Al_5W	*−9*	*0*	*−9*	[19]
	Al_4W	*−10.7*	*0*	*−10.7*	[19]
	Al_2S_3	−144.7	−5.84	−142.9	[17]
Ga	Ga_2S	−81.2	−14.9	−76.7	[56]
	GaS	−104.6	−7.7	−102.3	[56]
	Ga_2S_3	−102.7	−7.4	−100.5	[56]